RSC Advances

ROYAL SOCIETY OF CHEMISTRY

www.rsc.org/advances

Journal Name

RSCPublishing

ARTICLE

Syntheses, crystal structure, electrochemistry and luminescence properties of lanthano-germanotungstates

Cite this: DOI: 10.1039/xoxxoooooox

Received ooth January 2012,
Accepted ooth January 2012

DOI: 10.1039/xoxxoooooox

www.rsc.org/

Rakesh Gupta,[a] Firasat Hussain,[a*] J. N. Behera,[b] Amoassi Martin Bossoh,[c,d] Israël Martyr Mbomekalle[c] and Pedro de Oliveira[c]

[a]*Department of Chemistry, Faculty of Science, University of Delhi, Delhi – 110007*
[b]*School of Chemical Sciences, National Institute of Science Education and Research, Bhubaneswar, 751005*
[c]*Laboratoire de Chimie Physique, UMR 8000 CNRS, Université Paris-Sud, 91405 Orsay Cedex, France*
[d]*Université Félix Houphouët-Boigny, 01 BP V34 Abidjan 01, Côte d'Ivoire*

A series of sandwich type early lanthanoid substituted complexes: $[Ln(\alpha\text{-}GeW_{11}O_{39})_2]^{13-}$ [Ln = La^{III} (**La-1**) and Ce^{III} (**Ce-2**)] and acetate bridged hybrid dimeric complexes: $[\{Ln(\mu\text{-}CH_3COO)GeW_{11}O_{39}(H_2O)\}_2]^{12-}$ [Ln = Pr^{III} (**Pr-3**), Nd^{III} (**Nd-4**) and Sm^{III} (**Sm-5**)] were synthesized by the interaction of trilacunary $Na_{10}[GeW_9O_{34}]\cdot 18H_2O$ precursor with $Ln(NO_3)_3\cdot nH_2O$ in a potassium acetate buffer at pH 4.7. All these compounds were isolated as mixed alkali sodium/potassium salts and structurally characterised by various analytical techniques such as single crystal X-ray diffraction, FT-IR, ICP-AES, UV/vis, photoluminescence spectroscopy, thermo gravimetric analysis, ^{13}C and ^{1}H NMR spectroscopy, magnetism and electrochemistry. The FT-IR spectra suggest that compounds (**La-1a** and **Ce-2a**) and (**Pr-3a - Sm-5a**) are isomorphous. We also synthesized analogous acetate-bridged dimeic complexes (**Pr-3a** to **Sm-5a**) with mid and late lanthanoid ions (Ln = Eu^{III}, Gd^{III}, Tb^{III}, Dy^{III}, Ho^{III}, Er^{III}, Tm^{III} and Yb^{III}) using procedure published elsewhere and also investigated other studies such as electrochemistry, magnetic and photochromic properties. The molecular complexes **Pr-3a, Sm-5a, Eu-6a, Tb-8a, Dy-9a, Ho-10a, Er-11a** and **Tm-12a** show good photochromic behaviour at room temperature. The magnetic studies of **La-1a, Ce-2a, Pr-3a, Nd-4a** and **Sm-5a** were investigated at room temperature, and the molecular complexes show ferromagnetic behaviour.

Introduction

Polyoxometalates (POMs) are self-assemblies of oxometalates which are generally composed of early transition metals (Mo^{VI}, W^{VI}, V^{V}, Nb^{V} and Ta^{V}) in their highest oxidation states. POMs are a unique class of inorganic metal oxygen aggregates with large structural varieties and remarkable unexpected applications. Scientific interests in POM chemistry have attracted many researchers due to the discrete metal-oxo anions and versatile chemical, physical and biological properties. Lanthanoid cations are suitable for linking to POM anionic species due to their oxophilic nature and multiple coordination requirements. POMs exhibit good photochromic and redox behaviour in the presence of lanthanoid ions. Due to their interesting properties, POMs are very useful in the area of catalysis, medicine, molecular magnetism, imaging techniques, biotechnology and nanomaterial design.[1-9] The applications of POMs are primarily centred on their redox behaviour, photochemical response, ionic charge, conductivity and ionic weights. Well known Keggin and Wells-Dawson polyanions are generally stable in acidic solution, but upon increasing pH the hydrolytic cleavage of W=O bond occurs, which leads to the formation of well-defined lacunary species with mono, di, tri and multi lacunary type anions. These lacunary sites (voids) can be filled up by lanthanoid, transition metals or metal organic cationic species, allowing isolating functional materials.

Peacock and Weakley were the first to synthesize lanthanoid-containing sandwich type $[Ln^{III}W_{10}O_{35}]^{7-}$ polyanions which were characterised by elemental analysis.[10,11] Later, Weakley reported a sodium salt of decatungstocerate, which was structurally characterised by single crystal X-ray diffraction.[12] Since then, several groups have reacted lanthanoid ions with lacunary POM

precursors. Pope et al. reported a large cerium containing cyclic tungstoarsenate $[Ce_{16}As_{12}(H_2O)_{36}W_{148}O_{524}]^{76-}$ polyanion.[13] Later, Kortz et al.[14] reported another cerium containing tungstogermanate $[Ce_{20}Ge_{10}W_{100}O_{376}(OH)_4(H_2O)_{30}]^{56-}$. Recently Reinoso reported crown shaped cerium based 120-tungsto-12-germanate $[K\subset K_7Ce_{24}Ge_{12}W_{120}O_{456}(OH)_{12}(H_2O)_{64}]^{52-}$, subsequently they reported five crown-shaped large anions: the hexamers $[Na\subset Ln_{12}Ge_6W_{60}O_{228}(H_2O)_{24}]^{35-}$ (Ln = Pr^{III} and Nd^{III}) and $[K\subset Sm_{12}Ge_6W_{60}O_{228}(H_2O)_{22}]^{35-}$ and the dodecamers $[K\subset K_7Ln_{24}Ge_{12}W_{120}O_{444}(OH)_{12}(H_2O)_{64}]^{52-}$ (Ln=Pr^{III} and Nd^{III}).[15] We have isolated several examples of lanthanoid-substituted POM compounds with interesting properties. The $[Gd_8As_{12}W_{124}O_{432}(H_2O)_{22}]^{60-}$ complex is a gadolinium-containing octanuclear POM which has 124 tungsten centres.[16-25] Recently, Cronin and Kögerler reported few complexes which have more than 148 tungsten centres.[26] The chemistry of dimeric complexes of rare-earth-substituted $[Ln(XW_{11}O_{39})_2]$ (X = P^V and Si^{IV}) species is well known, but the germanotungstate family still remains elusive. Hervé and Tézé reported the monolacunary germanotungstate $[\alpha\text{-}GeW_{11}O_{39}]^{8-}$.[27] Later, Tourné synthesised a sandwich type uranium-containing $Cs_{12}[U(GeW_{11}O_{39})_2]\cdot 13\text{-}14H_2O$ germanotungstate.[28] Liu et al. reported a series of compounds with the general formula $K_{13}[Ln(GeW_{11}O_{39})_2]\cdot nH_2O$ (Ln = Ce^{III}, Pr^{III}, Nd^{III}, Sm^{III}, Eu^{III}, Gd^{III}, Tb^{III}, Dy^{III}, Tm^{III} and Yb^{III}) on the basis of powder X-ray diffraction (XRD), but no single crystal data was mentioned.[29] Later, Xu et al. reported a single crystal structure of the $K_{11.5}H_{1.5}[Pr(GeW_{11}O_{39})_2]\cdot 29H_2O$ compound in 2008.[30] The Wang group reported the isolation of three different types of polymeric structures: $[(CH_3)_4N]_2H_{1.50}[Nd_{1.50}(GeW_{11}O_{39})(H_2O)_6]\cdot 3H_2O$ and $[(CH_3)_4N]_2H_{2.25}[Sm_{1.25}(GeW_{11}O_{39})(H_2O)_4]\cdot 3.75H_2O$ having a zigzag chain, $[(CH_3)_4N]_{2.50}H_{2.50}[Y(GeW_{11}O_{39})(H_2O)_2]\cdot 4H_2O$ and $[(CH_3)_4N]_{2.50}H_{2.50}[Yb(GeW_{11}O_{39})(H_2O)_2]\cdot 3.75H_2O$ showing linear chain and $[Sm(H_2O)_7]_{0.5}H_{0.5}[Sm_2(GeW_{11}O_{39})(DMSO)_3(H_2O)_6]\cdot 3.5H_2O$ displaying a double parallel chainlike structure which was constructed by samarium cations.[31] Later, they synthesized similar compounds such as $[(CH_3)_4N]_{2.5}H_{7.5}[Eu(GeW_{11}O_{39})(H_2O)_2]_2\cdot 4.5H_2O$ and $[(CH_3)_4N]_2H_8[Tb(GeW_{11}O_{39})(H_2O)_2]_2\cdot 2.5H_2O$ which have one directional linear assembly, and $[Nd_{0.5}(H_2O)_2]H_{0.5}[Nd_2(GeW_{11}O_{39})(DMSO)_2(H_2O)_8]\cdot 5.5H_2O$ exhibiting double parallel chain like structure constructed through neodymium cations.[32] Khoshnavazi et al. reported the carbonate-encapsulated sandwich-type structures $[(A\text{-}\beta\text{-}GeW_9O_{34})_2(MOH_2)_3CO_3]^{13-}$ (M = Y^{3+}, Sm^{3+} and Yb^{3+}) in sodium carbonate solution.[33] Liu et al. reported the 2:1 and 1:1 polymeric structures: $Cs_3K[Eu_4(H_2O)_{18}Ge_2W_{22}O_{78}]\cdot 16.5H_2O$ and $Cs_3K_2[Eu(H_2O)_2GeW_{11}O_{39}]\cdot 10H_2O$, respectively, based on monovacant Keggin anion.[34] However, a few examples of the monovacant lanthanide-substituted Keggin-type organic-inorganic hybrid materials have been synthesised which was coordinated via the organic moiety.[35] For example, Yang et al. reported a series of double chain like organic–inorganic hybrid germanotungstates $[H_2dap][Cu(dap)_2]_{0.5}[Cu(dap)_2(H_2O)]\text{-}[Ln(H_2O)_3(\alpha\text{-}GeW_{11}O_{39})]\cdot 3H_2O$ (Ln = La^{III}, Pr^{III}, Nd^{III}, Sm^{III}, Eu^{III}, Tb^{III} and Er^{III}) (dap = 1,2-diaminopropane) in which 1-D polymeric assembly are linked together through $[Cu(dap)_2]^{2+}$ bridges and form Cu^{II}–Ln^{III} hetero-metallic double-chain architectures.[35f] Zhao et al. reported two 1D zigzag carboxylate-bridged copper–lanthanide organic-inorganic materials: $K_2[Cu(en)_2(H_2O)]_2\{[Cu(en)_2]_3[Ce(GeW_{11}O_{39})(H_2O)_2]_2(C_2O_4)\}\cdot 11H_2O$, formed by dimeric oxalate-bridging $\{[Cu(en)_2]_3[Ce(GeW_{11}O_{39})(H_2O)_2]_2(C_2O_4)\}^{6-}$ unit which was linked through $[Cu(en)_2]^{2+}$ cations, and $K_2[Cu(en)_2(H_2O)]_2\{[Cu(en)_2(H_2O)]_2[Tb(PW_{11}O_{39})(CH_3COO)(H_2O)]_2\}\cdot 15H_2O$ (en = 1,2-ethylenediamine) which displays a hybrid acetate-bridged dimeric structure $[(\alpha\text{-}PW_{11}O_{39})Tb(H_2O)(\eta^2,\mu\text{-}1,1)\text{-}CH_3COO]_2^{10-}$ which was constructed by $[Cu(en)_2(H_2O)]^{2+}$ fragments.[35g] Mialane et al. reported acetate-bridged silicotungstate with Gd^{III} and Yb^{III} rare earth cations, but no crystal structure was provided for the Gd^{III} complex.[36] One of us reported on similar complexes of yttrium-containing carboxylate-bridged silico and germanotungstates organic-inorganic hybrid materials.[19] Later, a series of organic-inorganic hybrid complexes with mid and late lanthanoid elements $[\{Ln(CH_3COO)GeW_{11}O_{39}(H_2O)\}_2]^{12-}$ (Ln = Eu^{III}, Gd^{III}, Tb^{III}, Dy^{III}, Ho^{III}, Er^{III}, Tm^{III}, and Yb^{III}), were synthesized in potassium acetate buffer at pH 4.7, but no chemistry was done with early lanthanoid cations, which still remained elusive.[21] Recently, we synthesised a series of rare-earth-substituted dimeric complexes of Keggin-type silicotungstates by a single step reaction in potassium acetate buffer at pH 4.5.[23]

Herein, we report the syntheses of two lanthanoid-substituted sandwich type complexes $[Ln(\alpha\text{-}GeW_{11}O_{39})_2]^{13-}$ [Ln = La^{III} and Ce^{III}] and three acetate bridged hybrid dimeric $[\{Ln(\mu\text{-}CH_3COO)GeW_{11}O_{39}(H_2O)\}_2]^{12-}$ [Ln = Pr^{III}, Nd^{III} and Sm^{III}] complexes, in potassium acetate buffer at pH 4.7, by using trilacunary $Na_{10}[GeW_9O_{34}]\cdot 18H_2O$ precursor.

Experimental section

Materials and analytical methods: The sodium salt of the trilacunary $Na_{10}[\alpha\text{-}GeW_9O_{34}]\cdot 18H_2O$ precursor was synthesized according to the literature procedure and confirmed by FT-IR spectroscopy.[27] All other chemicals were commercially purchased and used without further purification. Fourier transform infrared (FT-IR) spectra were recorded on a Perkin-Elmer BX spectrometer with KBr pellets. Liquid UV/vis spectra were recorded on an Analytic Jena Specord 250 spectrometer and solid UV/vis spectra were performed on a Thermo Scientific Evolution 300 spectrometer. Photoluminescence spectra were measured on a Fluorolog Horiba JobinYvon spectrometer. ^1H (at 400MHz) and ^{13}C-NMR (at 75MHz) spectra were recorded with a Jeol ECX 400P spectrometer in 9.38T field strength. Magnetic measurements were performed on a Micro sense (EV9) magnetometer from -22 to 22 kOe applied magnetic field. Thermogravimetric analysis (TGA) measurements were performed on a TG/DTA Instrument DTG-60 Shimadzu in the temperature range of 30-700 °C with a heating rate of 5 °C min^{-1} in a nitrogen atmosphere. Elemental analyses were performed on an ICP-AES instrument, ARCOS from M/s Spectro Germany. For the electrochemistry studies, pure water was obtained with a Milli-Q Intregral 5 purification set. All reagents were of high-purity grade and used as purchased without further purification: CH_3COOH

(Glacial, Prolabo Normapur) and $LiCH_3COO{\cdot}2H_2O$ (Acros Organics). The composition of the various media was 1.0 M $LiCH_3COO + CH_3COOH$ for pH 4.0, 5.0 and 6.0. The stability of all polyanions $[\{Ln(\mu\text{-}CH_3COO)GeW_{11}O_{39}(H_2O)\}_2]^{12-}$ (Ln = Pr^{III} (**Pr-3**), Nd^{III} (**Nd-4**), Sm^{III} (**Sm-5**), Eu^{III} (**Eu-6**), Tb^{III} (**Tb-8**), Dy^{III} (**Dy-9**), Ho^{III} (**Ho-10**), Er^{III} (**Er-11**), Tm^{III} (**Tm-12**) and Yb^{III} (**Yb-13**)) in solution as a function of the pH and time was studied by monitoring the evolution of their UV-visible spectra at least over 6 h. Such duration is long enough for the electrochemical characterisation of the compound and its possible application in electro-catalysis processes. These compounds were found to be stable in media having pH values ranging from 4 up to 6 at least. The UV-visible spectra were recorded on a Perkin-Elmer 750 spectrophotometer with 10^{-4} M solutions of the polyanion. Matched 2.00 mm optical path quartz cuvettes were used. Electrochemical data were obtained using an EG & G 273 A potentiostat driven by a PC with the M270 software. A one-compartment cell with a standard three-electrode configuration was used for cyclic voltammetry experiments. The reference electrode was a saturated calomel electrode (SCE) and the counter electrode platinum gauze of large surface area; both electrodes were separated from the bulk electrolyte solution via fritted compartments filled with the same electrolyte. The working electrodes were a 3 mm OD glassy carbon disc or a *c.a.* 10×10×2 mm^3 glassy carbon stick (Le Carbone-Lorraine, France). The pre-treatment of the first electrode before each experiment is adapted from a method described elsewhere.[37] The stick is polished twice with SiC paper, grit 500 (Struers). After each polishing step, the stick is rinsed and sonicated twice in Millipore water for a total of 10 minutes. Prior to each experiment, solutions were thoroughly de-aerated for at least 30 min with pure argon. A positive pressure of this gas was maintained during subsequent work. All cyclic voltammograms (CVs) were recorded at a scan rate of 10 mV s^{-1} and potentials are quoted against SCE unless otherwise stated. The polyanion concentration was 2×10^{-4} M. All the experiments were performed at room temperature. Results were very reproducible from one experiment to the other and slight variations observed over successive runs are rather attributed to the uncertainty associated with the detection limit of our equipment (potentiostat, hardware and software), and not to the working electrode pre-treatment nor to possible fluctuations in temperature.

Single-crystal structure determination: Single crystal structure data collection was performed on a Xcalibur Oxford diffractometer, operated at 50kV and 40mA (Mo-K_α radiation, λ = 0.71073 Å, graphite monochromated).[38] Pre-experiment, data collection, data reduction were performed with the Oxford program suite *CrysAlisPro*.[39] The structure was solved by direct methods using SHELXS-97[40] which readily revealed all the heavy atom positions (La, Ce, Pr, Nd, Sm, W and Ge) and enabled us to locate the other non-hydrogen (K, Na, O and C) positions from the difference Fourier maps. An empirical absorption correction based on symmetry equivalent reflections was applied using SCALE3 ABSPACK.[41] The last cycles of refinement included atomic positions, anisotropic thermal parameters for all the non-hydrogen atoms, and isotropic thermal parameters for all the hydrogen atoms. Full-matrix least-squares structure refinement against $|F^2|$ was carried out using the SHELXL-97[40] package of programs. Further details on the crystal structure data may be obtained from the Fachinformationszentrum Karlsruhe, 76344 Eggenstein-Leopoldshafen, Germany (fax: (+49) 7247-808-666; e-mail: crysdata@fiz-karlsruhe.de), on quoting the depository number CSD - 429591 for compound (**La-1a**) – 429592 for compound (**Ce-2a**) and the CCDC data can be obtained free of charge via http://www.ccdc.cam.ac.uk/conts/retrieving.html, or from the Cambridge Crystallographic Data Centre, 12 Union Road, Cambridge CB2 1EZ, UK; fax: (+44) 1223-336-033; or e-mail: deposit@ccdc.cam.ac.uk.on quoting the depository number CCDC - No – 1063248 for compound (**Pr-3a**), 1415074 for compound (**Sm-5a**) and 1415081 for compound (**Nd-4a**). Isolated oxygen atoms are crystal water and the considerable disorder of the cations and crystal water, which is a common phenomenon, encountered in polyoxometalate chemistry. For compounds **Pr-3a, Nd-4a** and **Sm-5a**, all hydrogen atoms were calculated after each cycle of refinement using a riding model, with C-H = 0.98 Å + U_{iso}(H) = 1.2U_{eq}(C) for methyl - H atoms.

Syntheses

Synthesis of $Na_3K_{10}[La(GeW_{11}O_{39})_2]{\cdot}27H_2O$ (La-1a)

In 25 mL of 1M potassium acetate buffer (pH 4.7) solution, 0.195 g (0.45mmol) of $La(NO_3)_3{\cdot}6H_2O$ and 0.526 g (0.15mmol) of $Na_{10}[\alpha\text{-}GeW_9O_{34}]{\cdot}18H_2O$ were added subsequently. The reaction mixture was continuously stirred at 60 °C for 1 hour. Then it was cooled at room temperature followed by its filtration. The filtrate was allowed to evaporate slowly at room temperature yielding a colourless needle crystalline product after 4-5 weeks. The crystalline material (compound **La-1a**) was collected and used for further analysis. Yield: 52.6% (on the basis of $Na_{10}[\alpha\text{-}GeW_9O_{34}]{\cdot}18H_2O$). FT-IR: (ν) = 947(s), 876(s), 813(s), 786(m), 755(m), 711(sh), 525(m), 459(sh), 443(w), 418(w) cm^{-1}. The number of crystal water molecules has been confirmed by TGA (%); calcd. for $27H_2O$ (found): 7.47 (7.55). Elemental analysis (%); calcd. for $Na_3K_{10}LaGe_2W_{22}O_{105}H_{54}$ (found): W 62.17 (63.08), Na 0.70 (0.99), K 6.59 (6.41).

Synthesis of $Na_3K_{10}[Ce(GeW_{11}O_{39})_2]{\cdot}28H_2O$ (Ce-2a)

Compound **Ce-2a** was synthesised following the above synthetic procedure by using 0.195 g (0.45mmol) of $Ce(NO_3)_3{\cdot}6H_2O$ instead of $La(NO_3)_3{\cdot}6H_2O$. Block type brown crystals were obtained, after about 4-5 weeks. Yield: 53.8% (on the basis of $Na_{10}[\alpha\text{-}GeW_9O_{34}]{\cdot}18H_2O$). FT-IR: (ν) = 947(s), 878(s), 812(s), 787(m), 755(m), 719(sh), 521(m), 461(sh), 442(w), 420(w) cm^{-1}. The number of crystal water molecules has been confirmed by TGA (%); calcd. for $28H_2O$ (found): 7.72 (7.66). Elemental analysis (%); calcd. for $Na_3K_{10}CeGe_2W_{22}O_{106}H_{56}$ (found): W 61.98 (62.76), Na 1.40 (0.95), K 5.38 (6.45).

Synthesis of $Na_6K_6[\{Pr(\mu\text{-}CH_3COO)GeW_{11}O_{39}(H_2O)\}_2]{\cdot}25H_2O$ (Pr-3a)

Compound **Pr-3a** was synthesised following the above synthetic procedure by using 0.196 g (0.45mmol) of $Pr(NO_3)_3{\cdot}6H_2O$ instead of

$La(NO_3)_3{\cdot}6H_2O$. Greenish diamond-shaped crystals were obtained after about 4-5 weeks. Yield: 55.7% (on the basis of $Na_{10}[\alpha\text{-}GeW_9O_{34}]{\cdot}18H_2O$). FT-IR: (ν) = 1628(s), 1525(s), 1427(s), 1404(w), 951(s), 892(s), 805(s), 745(w), 691(sh), 670(m), 527(m), 498(w), 464(m), 448(w), 419(w), 412(w) cm^{-1}. The number of crystal water molecules has been confirmed by TGA (%); calcd. for $25H_2O$ (found): 7.22 (7.09). Elemental analysis (%); calcd. for $Na_6K_6Pr_2Ge_2W_{22}O_{109}H_{60}C_4$ (found): W 60.12 (60.78), Na 2.05 (1.86), K 3.48 (4.11).

Synthesis of $Na_4K_8[\{Nd(\mu\text{-}CH_3COO)GeW_{11}O_{39}(H_2O)\}_2]{\cdot}22H_2O$ (Nd-4a)

Compound **Nd-4a** was synthesised following the above synthetic procedure by using 0.197 g (0.45mmol) of $Nd(NO_3)_3{\cdot}6H_2O$ instead of $La(NO_3)_3{\cdot}6H_2O$. Violet diamond-shaped crystals were obtained after about 4-5 weeks. Yield: 56.2% (on the basis of $Na_{10}[\alpha\text{-}GeW_9O_{34}]{\cdot}18H_2O$). FT-IR: (ν) = 1630(s), 1525(s), 1430(s), 1401(w), 950(s), 893(s), 805(s), 744(m), 690(sh), 674(w), 528(m), 498(w), 464(m), 448(w), 414(w), 409(w) cm^{-1}. The number of crystal water molecules has been confirmed by TGA (%); calcd. for $22H_2O$ (found): 6.47 (6.30). Elemental analysis (%); calcd. for $Na_4K_8Nd_2Ge_2W_{22}O_{106}H_{54}C_4$ (found): W 60.54 (61.15), Na 1.38 (1.06), K 4.67 (5.43).

Synthesis of $Na_3K_9[\{Sm(\mu\text{-}CH_3COO)GeW_{11}O_{39}(H_2O)\}_2]{\cdot}19H_2O$ (Sm-5a)

Compound **Sm-5a** was synthesised following the above synthetic procedure by using 0.200 g (0.45mmol) of $Sm(NO_3)_3{\cdot}6H_2O$ (0.45mmol) instead of $La(NO_3)_3{\cdot}6H_2O$. Slightly bluish diamond-shaped crystals were obtained after about 4-5 weeks. Yield: 58.9% (on the basis of $Na_{10}[\alpha\text{-}GeW_9O_{34}]{\cdot}18H_2O$). FT-IR: (ν) = 1629(s), 1525(s), 1436(s), 1400(w), 951(s), 894(s), 807(s), 747(w), 692(sh), 676(m), 528(m), 499(w), 465(m), 449(w), 420(w), 412(w) cm^{-1}. The number of crystal water molecules has been confirmed by TGA (%); calcd. for $19H_2O$ (found): 5.69 (5.67). Elemental analysis (%); calcd. for $Na_3K_9Sm_2Ge_2W_{22}O_{103}H_{48}C_4$ (found): W 60.92 (60.85), Na 1.04 (0.93), K 5.29 (5.81).

We have also synthesised similar acetate-bridged germanotungstates: $[\{Ln(\mu\text{-}CH_3COO)GeW_{11}O_{39}(H_2O)\}_2]^{12-}$ (Ln = Eu^{III} (**Eu-6**), Gd^{III} (**Gd-7**), Tb^{III} (**Tb-8**), Dy^{III} (**Dy-9**), Ho^{III} (**Ho-10**), Er^{III} (**Er-11**), Tm^{III} (**Tm-12**) and Yb^{III} (**Yb-13**)) complexes with mid and late lanthanoid cations according to previous literature procedure and compounds were confirmed by FT-IR spectroscopy.[21] The photoluminescence properties of these synthesised compounds were studied at room temperature.

Results and discussion

Syntheses and structure

All the title molecular complexes **1a - 5a** were synthesised in a single step reaction procedure by reacting a trilacunary $Na_{10}[\alpha\text{-}GeW_9O_{34}]{\cdot}18H_2O$ precursor with $Ln(NO_3)_3{\cdot}nH_2O$ in potassium acetate buffer (pH 4.7) solution. All the compounds were isolated as mixed alkali sodium/potassium salts for analyses. We have obtained two types of complexes with $Na_{10}[\alpha\text{-}GeW_9O_{34}]{\cdot}18H_2O$ precursor, of which either a La^{III} or a Ce^{III} cation formed sandwich-type species without bridging acetate and the Pr^{III}, Nd^{III} or Sm^{III} cations formed acetate bridged hybrid dimeric complexes.

Single crystal X-ray diffraction studies of the **La-1a** and **Ce-2a** molecular complexes show that each of the lanthanoid (La^{III} and Ce^{III}) cation is sandwiched between two monolacunary $[\alpha\text{-}GeW_{11}O_{39}]^{8-}$ units, which act as tetradentate ligands. Four oxygen atoms of each unit are coordinated with the lanthanoid cation. Thus, the lanthanoid cation is eight-coordinated and situated in the square antiprismatic geometry (see **fig. 1**).

In the same reaction conditions the Pr^{III}, Nd^{III} and Sm^{III} cations with the $Na_{10}[\alpha\text{-}GeW_9O_{34}]{\cdot}18H_2O$ salt formed acetate bridged hybrid dimeric species. Single crystal X-ray diffraction analysis shows that the **Pr-3a**, **Nd-4a**, and **Sm-5a** compounds are isostructural and crystallised in the monoclinic crystal system with space group $P2_1/c$. The structure of the title polyanion is same as that of a series of germanotungstates with mid and late lanthanoid salts reported by one of us.[21] The trilacunary Keggin $[\alpha\text{-}GeW_9O_{34}]^{10-}$ anion starting material easily transforms to the monolacunary $[\alpha\text{-}GeW_{11}O_{39}]^{8-}$ anion at acidic pH (4.7). The formation of the $[\alpha\text{-}GeW_{11}O_{39}]^{8-}$ anion indicates that fragmentation of the $[\alpha\text{-}GeW_9O_{34}]^{10-}$ starting material occurred during the course of the reaction. The title polyanion is the self-assembly of two lanthanoid cations, two acetate ligands and two monolacunary ($\alpha\text{-}GeW_{11}O_{39}$) units in addition to two water molecules which are coordinated to the lanthanoid centre. Two lanthanoid cations are linked together through two acetate ligands in a $\mu_2{:}\eta^2\text{-}\eta^1$ manner and form the $[\{Ln(CH_3COO)\}_2]^{4+}$ cationic species which further reacts with monolacunary Keggin $[\alpha\text{-}GeW_{11}O_{39}]^{8-}$ anions. Each lanthanoid cation of the polyanion is eight-coordinated and has a square antiprismatic geometry. The coordination environment of the lanthanoid is satisfied with four oxygen atoms of the monolacunary Keggin $[\alpha\text{-}GeW_{11}O_{39}]^{8-}$ anion, three oxygen atoms of the acetate ligands and one terminal water molecule (see **fig. 2**).

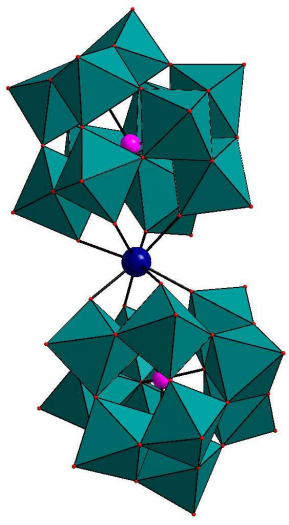

Fig. 1 Ball and Polyhedron representation of the polyanion $[Ln(GeW_{11}O_{39})_2]^{13-}$ [Ln = La^{III} (**La-1**) and Ce^{III} (**Ce-2**)] (Color code:

dark blue ball: lanthanoid; teal polyhedron: tungsten; pink ball: germanium; red ball: oxygen).

Table 1. Crystallographic data for the compounds **La-1a, Ce-2a**, **Pr-3a**, **Nd-4a**, and **Sm-5a**.

Compounds	**La-1a**	**Ce-2a**	**Pr-3a**	**Nd-4a**	**Sm-5a**
Empirical Formula	$K_{11.30}Na_{0.50}Ge_2LaO_{95}W_{22}$	$K_{9.50}Na_6Ge_2CeO_{93}W_{22}$	$C_4H_6K_8Na_6Ge_2Pr_2O_{108}W_{22}$	$C_4H_6K_8Na_4Ge_2Nd_2O_{101}W_{22}$	$C_4H_6K_8Na_6Ge_2Sm_2O_{108}W_{22}$
FW	6302.11	6327.39	6704.53	6553.21	6723.41
Crystal system	Triclinic	Triclinic	Monoclinic	Monoclinic	Monoclinic
Space group	P-1	P-1	$P2_1/c$	$P2_1/c$	$P2_1/c$
a/Å	12.8237(3)	12.694(2)	20.2531(4)	20.0790(7)	20.2068(6)
b/Å	16.7219(5)	16.602(2)	12.7325(3)	12.5625(4)	12.6869(3)
c/Å	23.1953(6)	23.0874(18)	21.2946(5)	21.1756(7)	21.2464(5)
α[^{0}]	94.455(2)	94.553(9)	90.000	90.000	90.000
β(^{0})	99.385(2)	100.150(15)	110.677(2)	111.010(4)	110.760(3)
γ[^{0}]	92.586(2)	91.19(2)	90.000	90.000	90.000
V/Å^3	4884.1(2)	4771.3(11)	5093.1(2)	4986.3(3)	5093.1(2)
Z	2	2	2	2	2
T/K	293(2)	298(2)	283(2)	298(2)	298(2)
ρ_{calcd}[g cm^{-3}]	4.285	4.404	4.372	4.365	4.384
μ/mm^{-1}	27.410	28.032	26.719	27.337	26.915
Gof(on F^2)	1.054	1.069	1.109	1.067	1.153
F(000)	5458	5481	5844	5692	5856
Ref. collected	62783	63399	66677	62926	66636
Unique (Rint)	15331	15015	7935	9444	8580
Observed[$I>2\sigma(I)$]	18538	18101	9666	6597	9666
Parameters	707	702	712	712	712
R_1[I >2σ(I)][a]	0.0591	0.0610	0.0456	0.0625	0.0380
R_w (all data)[b]	0.1562	0.1578	0.0926	0.1292	0.0804

[a] $R_1 = \sum||F_o| - |F_c|| / \sum|F_o|$. [b] $R_w = [\sum w(F_o^2 - F_c^2)^2 / \sum w(F_o^2)^2]^{1/2}$

Recently, we reported a series of dimeric acetate-bridged $[\{Ln(\alpha\text{-}SiW_{11}O_{39})(H_2O)\}_2(\mu\text{-}CH_3COO)_2]^{12-}$ (Ln = Eu^{III}, Gd^{III}, Tb^{III}, Dy^{III}, Ho^{III}, Er^{III} and Tm^{III}) and three $[Ln(\alpha\text{-}SiW_{11}O_{39})_2]^{13-}$ (Ln = Pr^{III}, Nd^{III} and Sm^{III}) silicotungstates.[23] Here, it is very interesting to note that the Pr^{III} and Nd^{III} analogous silicotungstates formed sandwich-type species without bridging acetates, whereas we obtained acetate-bridged germanotungstates with the same lanthanoids in potassium acetate buffer solution at pH 4.7. This may be due to the fact that the $[\alpha\text{-}GeW_{11}O_{39}]^{8-}$ anion has a larger open angle in the vacant site than the $[\alpha\text{-}SiW_{11}O_{39}]^{8-}$ anion.

The Niu and Wang's group synthesised a series of analogous acetate-bridged phosphotungstic complexes $[\{(\alpha\text{-}PW_{11}O_{39})Ln(H_2O)(\eta^2,\mu\text{-}1,1)\text{-}CH_3COO\}_2]^{10-}$ (Ln = Sm^{III}, Eu^{III}, Gd^{III}, Tb^{III}, Ho^{III} and Er^{III}) in which the Sm^{III} cation formed acetate-bridged organic-inorganic hybrid compound.[42] The synthesis of the **Pr-3a** polyanion was dependent on the heating time. The compound obtained when the reaction mixture was heated to 60 °C for 30 minutes had no bridging acetates, but **Pr-3a** formed when the heating lasted for 1 h, resulting in acetate-bridged diamond-shaped crystals.

Generally, the average bond lengths of Ln–O follow a decreasing order across the series i.e. upon increasing the ionic radius of lanthanoid (see **Table S1** and fig. **S2**). This trend was in accordance with lanthanoid contraction.

Bond Valence Sum (BVS) calculations[43] show that neither the oxygen atoms of the two (α-$GeW_{11}O_{39}$) units in the title compounds nor the bridging oxygen atoms Ln-O-W are protonated. Two terminal water molecules were found on the

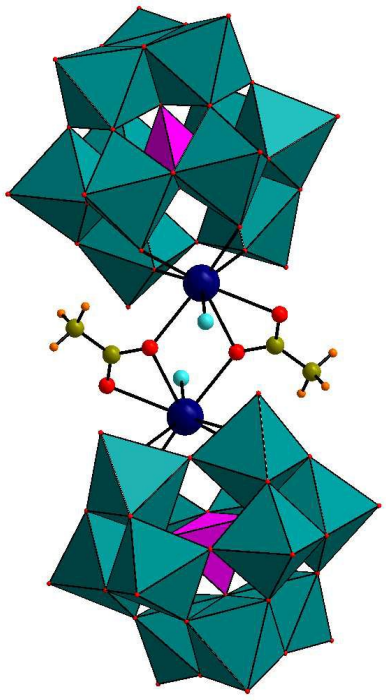

Fig. 2 Ball and polyhedron representation of the polyanion $[\{Ln(\mu\text{-}CH_3COO)GeW_{11}O_{39}(H_2O)\}_2]^{12-}$ [Ln = Pr^{III} (**Pr-3**), Nd^{III} (**Nd-4**) and Sm^{III} (**Sm-5**)] (Color code: dark blue ball: lanthanoid; teal polyhedron: tungsten; pink polyhedron: germanium; red ball: oxygen; dark yellow ball: carbon; orange ball: Hydrogen; aqua ball: water molecule).

lanthanoid atoms in the **Pr-3a** to **Sm-5a** POMs. So, the net charge of the title polyanions **Pr-3a** to **Sm-5a** is 12- and that of **La-1a** and **Ce-2a** is 13-, being compensated by alkali sodium and potassium cations in the solid state.

FT-IR spectroscopy

The FT-IR spectra of the title polyanions **La-1a**, **Ce-2a**, **Pr-3a**, **Nd-4a**, and **Sm-5a** were recorded on KBr pellets with a Perkin-Elmer BX spectrometer. The FT-IR spectra of the **La-1a** and **Ce-2a** show almost similar frequencies in the range 1800-400 cm^{-1}. The band in the range 876-878 cm^{-1} is assigned to ν_{as}(Ge-O_a) and that around 947 cm^{-1} is attributed to the antisymmetric stretching vibration of the terminal ν_{as}(W-O_t). Bands at wavenumbers 786 or 787 cm^{-1} and 755 cm^{-1} are due to vibrations corresponding to the corner sharing ν_{as}(W-O_b-W) and bands at 755 cm^{-1} and in the range 711-719 cm^{-1} are attributed to the antisymmetric stretching vibration of the edge sharing ν_{as}(W-O_c-W). The FT-IR spectra show that the compounds **Pr-3a**, **Nd-4a** and **Sm-5a** have similar characteristic antisymmetric stretching vibrations in the region 1800-400 cm^{-1} with slightly shifts in the position of the vibration bands. These three compounds exhibit four characteristic antisymmetric stretching vibrations in the fingerprint region (1000 to 400 cm^{-1}) of the POM ligands which are attributed to antisymmetric stretching modes of ν_{as}(Ge-O_a), terminal ν_{as}(W-O_t), corner sharing ν_{as}(W-O_b-W) and edge sharing ν_{as}(W-O_c-W). In the FT-IR spectra, bands in between 892-894 cm^{-1} are assigned to ν_{as}(Ge-O_a) and the band at 950 or 951 cm^{-1} corresponds to the antisymmetric stretching vibrations of ν_{as}(W-O_t). This band is almost not shifted in these polyanions, suggesting that the cations have little influence on the terminal oxygen atoms of the $[\alpha\text{-}GeW_{11}O_{39}]^{8-}$ fragments, and it is considered as pure vibrations of the POM ligands. Bands in the range of 805-807 cm^{-1} and 744-747 cm^{-1} are attributed to ν_{as}(W-O_b-W) and wavenumbers at 691 or 692 cm^{-1} and in between 670-676 cm^{-1} are due to the antisymmetric stretching vibrations of ν_{as}(W-O_c-W). Furthermore, four antisymmetric stretching modes in the range 1630-1400 cm^{-1} are attributed to the ν_{as}(C=O) and ν_{as}(C-O) group of the acetate ligands which are bridging the metal centres in a μ_2: η^2-η^1 manner.[21,23,44]

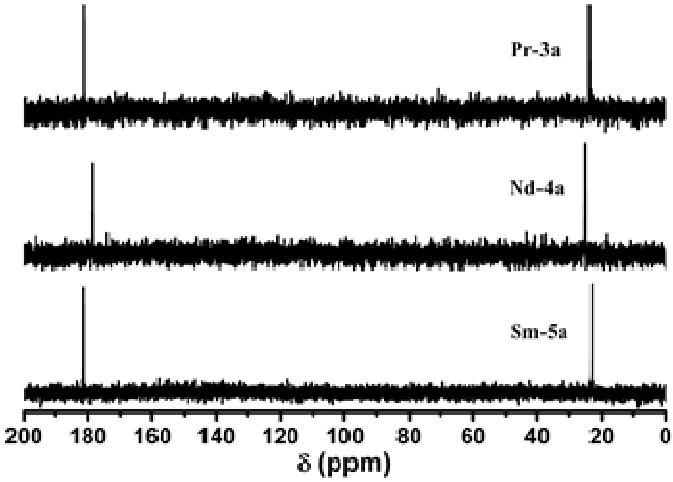

Fig. 3 ^{13}C-NMR spectra of the **Pr-3a**, **Nd-4a**, and **Sm-5a** POMs.

NMR spectroscopy

The ^{1}H (at 400MHz) and ^{13}C NMR (at 75MHz) spectra of the **Pr-3a**, **Nd-4a**, and **Sm-5a** compounds were recorded in a field of 9.38 T at 298 K. The samples were prepared by dissolving the isolated crystals in D_2O. In the ^{13}C NMR spectra two well separated signals are observed with an intensity ratio of 1:1 which are the result of the methyl and the carboxylic carbon atoms of the acetate ligands. These signals are located at δ = 23.89 and 181.33 ppm for **Pr-3a**, at δ = 24.92 and 178.34 ppm for **Nd-4a** and at δ = 23.11 and 181.56 ppm for **Sm-5a**. Downfield ^{13}C NMR signal is due to the oxygen-bound carbon atoms of the carboxylic groups (see **fig. 3**).

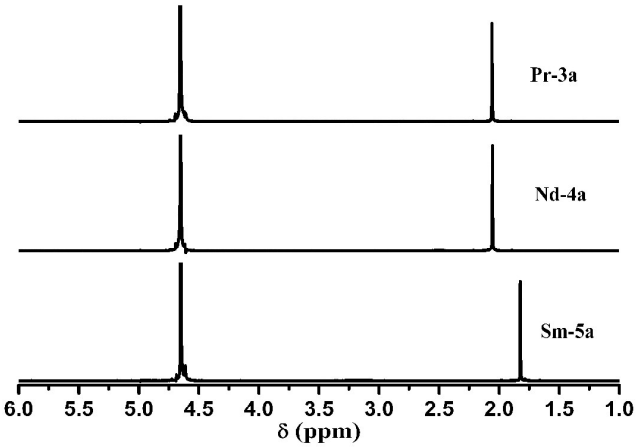

Fig. 4 ^{1}H-NMR spectra of the **Pr-3a**, **Nd-4a**, and **Sm-5a** POMs

The ^{1}H NMR spectra of the **Pr-3a**, **Nd-4a**, and **Sm-5a** compounds show two signals at δ = 2.06 and 4.65 ppm for **Pr-3a**, at δ = 2.05 and 4.65 ppm for **Nd-4a** and at δ = 1.82 and 4.65 ppm for **Sm-5a** in which the former signal is due to the protons of the methyl groups and the latter one is for the protons of the water molecules (see **fig. 4**).[19,23] In the series from La to Sm, number of unpaired electrons is increased hence the up field shielding increases which further effect the NMR signals. Hence the value of Sm is 1.82 as compared to Pr (2.06) and Nd (2.05).

UV/vis spectroscopy

The UV/vis spectra of all the molecular clusters were recorded in aqueous solution in the range 190-800 nm. In this range, the compounds show two characteristic absorption bands: a strong band centered in the range 190-200 nm and a broad, weak band at around 256 nm. The higher energy absorption band (190-200 nm) was attributed to the pπ-dπ charge transfer transition of the $O_t \rightarrow W$ bond and the lower energy absorption band (256 nm) is due to the pπ-dπ charge transfer transition of the $O_{b,c} \rightarrow W$ bond (see **fig. S6**).[23,25] We successfully recorded the solid state UV/vis spectrum of the **Pr-3a**, **Nd-4a**, **Sm-5a**, **Dy-9a**, **Ho-10a**, **Er-11a** and **Tm-12a** POMs.

The solid-state absorption spectrum of **Pr-3a** shows four intense relatively broad absorption bands at around 449, 473, 488 and 599 nm in the visible region. These bands are observed due to the transitions of the $^{3}H_4$ ground state to the $^{3}P_2$, $^{3}P_1$, $^{3}P_0$ and $^{1}D_2$ excited states of the Pr^{III} ion, respectively. The most intense $^{3}H_4 \rightarrow {}^{3}P_2$ transition is responsible for the violet-blue colour of the **Pr-3a** compound (see **fig. 5**).[45]

The absorption spectrum of the **Nd-4a** compound shows six absorption bands at around 515, 528, 586, 628, 686 and 749 nm in the visible region, and two bands at 804 and 874 nm in the near IR region, corresponding to the $^{4}I_{9/2} \rightarrow {}^{2}K_{13/2}$, $^{4}I_{9/2} \rightarrow {}^{4}F_{5/2}$, $^{4}I_{9/2} \rightarrow {}^{4}F_{3/2}$, $^{4}I_{9/2} \rightarrow {}^{2}H_{11/2}$, $^{4}I_{9/2} \rightarrow {}^{4}F_{9/2}$, $^{4}I_{9/2} \rightarrow {}^{4}I_{15/2}$, $^{4}I_{9/2} \rightarrow {}^{4}I_{13/2}$ and $^{4}I_{9/2} \rightarrow {}^{4}I_{11/2}$ transitions of the Nd^{III} ion (see **fig. S7**).[42,45c] In the absorption spectrum of the **Sm-5a** species, nine absorption bands are found due to the transitions from the ground state $^{6}H_{5/2}$ to various higher energy levels. Two bands are observed in the UV region at about 377 and 389 nm due to the transitions $^{6}H_{5/2} \rightarrow {}^{4}D_{1/2}$ and $^{6}H_{5/2} \rightarrow {}^{4}G_{11/2}, {}^{4}H_{11/2}$, respectively, whereas seven absorption bands are observed in the visible region at around 405, 420, 442, 465, 481, 502 and 532 nm which are assigned to the $^{6}H_{5/2} \rightarrow {}^{4}K_{11/2}$, $^{6}H_{5/2} \rightarrow {}^{5}P_{3/2}, {}^{5}P_{5/2}$, $^{6}H_{5/2} \rightarrow {}^{4}G_{9/2}, {}^{4}I_{15/2}$, $^{6}H_{5/2} \rightarrow {}^{4}F_{5/2}, {}^{4}M_{17/2}$, $^{6}H_{5/2} \rightarrow {}^{4}I_{11/2}, {}^{4}I_{13/2}$, $^{6}H_{5/2} \rightarrow {}^{4}G_{7/2}$ and $^{6}H_{5/2} \rightarrow {}^{4}F_{3/2}$ transitions of the Sm^{III} ion, respectively. The strongest absorption band is found at 405 nm due to the $^{6}H_{5/2} \rightarrow {}^{4}K_{11/2}$ transition (see **fig. S8**).[45c,46]

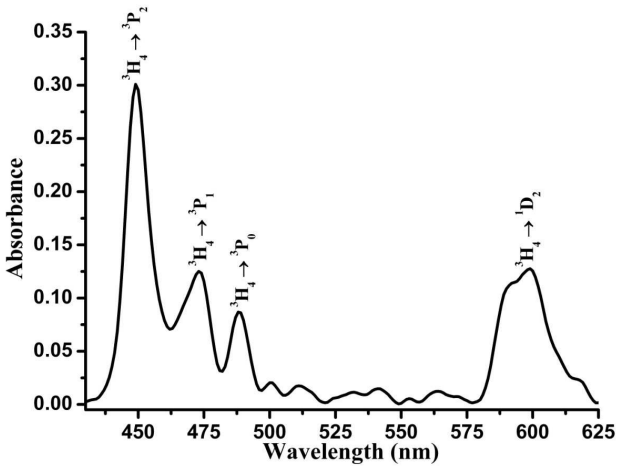

Fig. 5 Solid state UV/vis spectrum of **Pr-3a** POM.

The **Dy-9a** compound displays eight bands in the absorption spectrum. These four weak intensity bands are observed in the visible region at 389, 427, 452 and 475 nm and ascribed to the $^{6}H_{15/2} \rightarrow {}^{4}F_{7/2}, {}^{4}I_{13/2}$, $^{6}H_{15/2} \rightarrow {}^{4}F_{9/2}$, $^{6}H_{15/2} \rightarrow {}^{4}I_{15/2}$ and $^{6}H_{15/2} \rightarrow {}^{4}G_{11/2}$ transitions, respectively, and four relatively higher intensity bands at around 759, 810, 913 and 998 nm towards the near IR region. These are assigned to the $^{6}H_{15/2} \rightarrow {}^{6}F_{3/2}$, $^{6}H_{15/2} \rightarrow {}^{6}F_{5/2}$, $^{6}H_{15/2} \rightarrow {}^{6}F_{7/2}$ and $^{6}H_{15/2} \rightarrow {}^{6}H_{5/2}$ transitions of the Dy^{III} ion (see **fig. S9**).[45b,45c,47]

For the **Ho-10a** compound, seven bands are observed at around 387, 419, 454, 472, 488, 541 and 647 nm in the absorption spectrum. These bands are attributed to the $^{5}I_8 \rightarrow {}^{5}G_4$, $^{5}I_8 \rightarrow {}^{5}G_5$, $^{5}I_8 \rightarrow {}^{5}F_1, {}^{5}G_6$, $^{5}I_8 \rightarrow {}^{3}K_8, {}^{5}F_2$, $^{5}I_8 \rightarrow {}^{5}F_3$, $^{5}I_8 \rightarrow {}^{5}F_4, {}^{5}S_2$ and $^{5}I_8 \rightarrow {}^{5}F_6$ transitions of the Ho^{III} ion. The $^{5}I_8 \rightarrow {}^{5}F_4, {}^{5}S_2$ and $^{5}I_8 \rightarrow {}^{5}G_6$ transitions contribute to the colour of this species (see **fig. 6a**).[45c,46] Eight bands are observed in the absorption spectrum of the **Er-11a** compound, which are centred at 380, 408, 452, 490, 524, 546, 655 and 804 nm. These bands are attributed to appropriate f-f electronic transitions of the Er^{III} ion from the $^{4}I_{15/2}$ ground state to the following excited states: $^{4}G_{11/2}$, $^{2}H_{9/2}$, $^{4}F_{3/2,5/2}$, $^{4}F_{7/2}$, $^{2}H_{11/2}$, $^{4}S_{3/2}$, $^{4}F_{9/2}$ and $^{4}I_{9/2}$, respectively. Although the Er^{III} ion has several relatively intense absorption bands in the visible region of the spectrum, its pink colour is almost entirely due to the $^{4}I_{15/2} \rightarrow {}^{2}H_{11/2}$ transition at 524 nm in the green region (see **fig. 6b**).[46,48] The **Tm-12a** compound shows four intense

absorption bands in the visible region that are seen at 471, 668, 689 and 799 nm. These bands are due to excitations from the $^3H_6$ ground state to the different higher energy levels $^1G_4$, $^3F_2$, $^3F_3$ and $^3F_4$ of the Tm^{III} ion, respectively (see **fig. S10**).[45b]

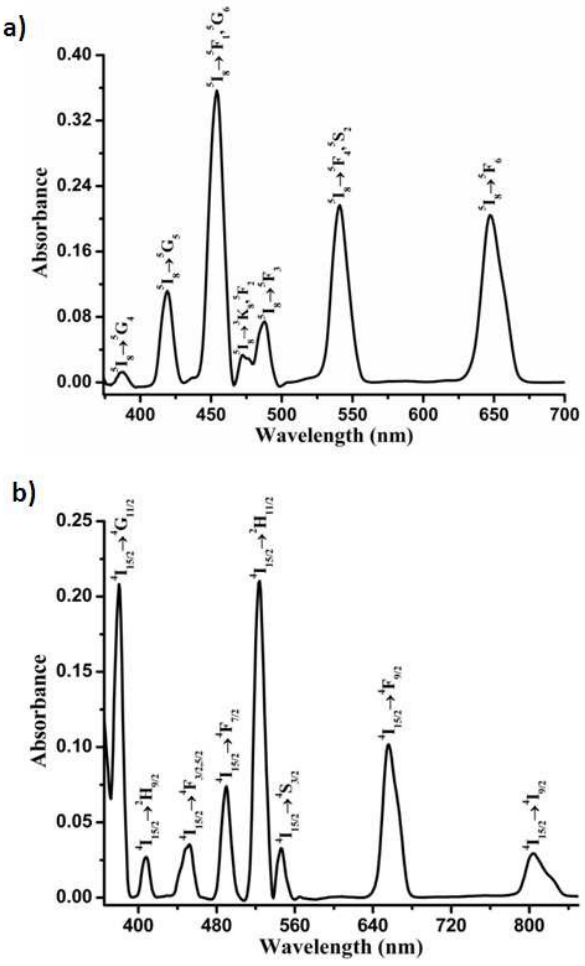

Fig. 6 Solid-state UV/vis spectrum of (a) **Ho-10a** and (b) **Er-11a.**

Photoluminescence spectroscopy

The emission spectrum of the **Pr-3a** compound upon photo-excitation at 450 nm displays six emission peaks in the visible region at about 533, 593, 606, 620, 650 and 697 nm at room temperature. Peaks are ascribed to the $^3P_0 \rightarrow {}^3H_5$, $^3P_1 \rightarrow {}^3H_6$, $^1D_2 \rightarrow {}^3H_4$, $^3P_0 \rightarrow {}^3H_6$, $^3P_0 \rightarrow {}^3F_2$ and $^3P_0 \rightarrow {}^3F_3$ & $^3P_1 \rightarrow {}^3F_4$ transitions of the Pr^{III} ion. The intense emission peak at 606 nm ($^1D_2 \rightarrow {}^3H_4$) is responsible for the red emission of the **Pr-3a** species (see **fig. S11**).[45b,49] The photo-excitation of the compound **Sm-5a** at 377 nm shows four characteristic emission peaks in the visible region at 565, 601, 648 and 708 nm, which are assigned to transitions from the $^4G_{5/2}$ excited energy level of the Sm^{III} ion to different ground state energy levels, $^6H_{5/2}$ (zero-zero band), $^6H_{7/2}$ (magnetic dipole transition), $^6H_{9/2}$ (electric dipole transition) and $^6H_{11/2}$, respectively. The Sm^{III} ion exhibits a more intense deep-red colour due to a relatively stronger $^4G_{5/2} \rightarrow {}^6H_{9/2}$ electrical dipole emission than the orange $^4G_{5/2} \rightarrow {}^6H_{7/2}$ magnetic dipole or the green $^4G_{5/2} \rightarrow {}^6H_{5/2}$ emission (see **fig. 7a**).[46,49a,50]

The emission spectrum of the **Eu-6a** species consists of a series of six peaks situated at about 545 (green), 580 (yellow), 593 (orange), 619 (red), 651 (deep-red) and 699 (deep-red) nm on the photo-excitation at 394 nm. These peaks originate from the $^5D_1 \rightarrow {}^7F_1$, $^5D_0 \rightarrow {}^7F_0$, $^5D_0 \rightarrow {}^7F_1$, $^5D_0 \rightarrow {}^7F_2$, $^5D_0 \rightarrow {}^7F_3$ and $^5D_0 \rightarrow {}^7F_4$ electronic transitions respectively. The $^5D_0 \rightarrow {}^7F_{1,3}$ are magnetic-dipolar transitions, which are independent from their local environments, and the intensity of the $^5D_0 \rightarrow {}^7F_1$ transition varies with the ligand field strength acting on Eu^{III} ion. The $^5D_0 \rightarrow {}^7F_{0,2,4}$ transitions are electric-dipolar ones, being sensitive to their local environment. The $^5D_0 \rightarrow {}^7F_2$ transition is extremely sensitive to the chemical bonds in the vicinity of the Eu^{III} ion and its intensity increases as the Eu^{III} ion site symmetry decreases. As a consequence, the ratio of intensities of the hypersensitive electric dipole transition $^5D_0 \rightarrow {}^7F_2$ (red emission, $\Delta J=2$) over the less sensitive magnetic dipole transition $^5D_0 \rightarrow {}^7F_1$ (orange emission) is commonly used as a measure of the coordination state and site symmetry of the Eu^{III} ion. In the present case, the intensity ratio $I(^5D_0 \rightarrow {}^7F_2)/I(^5D_0 \rightarrow {}^7F_1)$ is equal to 3.87, which indicates that the symmetry of the Eu^{III} ion is low. The intense $^5D_0 \rightarrow {}^7F_2$ transition is responsible for the red emission of the **Eu-6a** compound. The $^5D_0 \rightarrow {}^7F_0$ transition is symmetry forbidden in a field of symmetry and indicates that the Eu^{III} ions in the POMs occupy low symmetry sites without an inversion centre, which is in good accordance with the present results and further can be correlated with previous results (see **fig. 7b**).[22,45b,51] The **Tb-8a** compound emits green photoluminescence at room temperature upon photo-excitation at 330 nm. The emission spectrum of **Tb-8a** exhibits four characteristic emission peaks at 492, 547, 586 and 622 nm, which are assigned to the $^5D_4 \rightarrow {}^7F_6$, $^5D_4 \rightarrow {}^7F_5$, $^5D_4 \rightarrow {}^7F_4$ and $^5D_4 \rightarrow {}^7F_3$ transitions, respectively. The $^5D_4 \rightarrow {}^7F_6$ transition is a magnetic dipole one and its intensity varies with the ligand field strength on the Tb^{III} ion. This $^5D_4 \rightarrow {}^7F_6$ transition does not split. The higher intensity peak $^5D_4 \rightarrow {}^7F_5$ is an electric dipole transition that is sensitive to changes in the chemical bonds in the vicinity of the Tb^{III} ion. Its intensity increases when the site symmetry of the Tb^{III} ion decreases. Thus, the intensity ratio $I(^5D_4 \rightarrow {}^7F_5)/I(^5D_4 \rightarrow {}^7F_6)$ is used to determine the coordination state and site symmetry of the Tb^{III} ion. In this case, the intensity ratio of the $I(^5D_4 \rightarrow {}^7F_5)/I(^5D_4 \rightarrow {}^7F_6)$ is equal to 5.15 (see **fig. 8a**).[42,47,52] Upon excitation at 370 nm, the **Dy-9a** species shows three emission peaks at 484 (blue), 576 (yellow) and 664 (red) nm which are ascribed to the characteristic $^4F_{9/2} \rightarrow {}^6H_{15/2}$, $^4F_{9/2} \rightarrow {}^6H_{13/2}$ and $^4F_{9/2} \rightarrow {}^6H_{11/2}$ transitions of the Dy^{III} ion, respectively. A higher intensity, hypersensitive, yellow emission ($^4F_{9/2} \rightarrow {}^6H_{13/2}$) transition with $\Delta J=2$ is strongly influenced by the chemical environment of the Dy^{III} ions (see **fig. 8b**).[45b,47,49a]

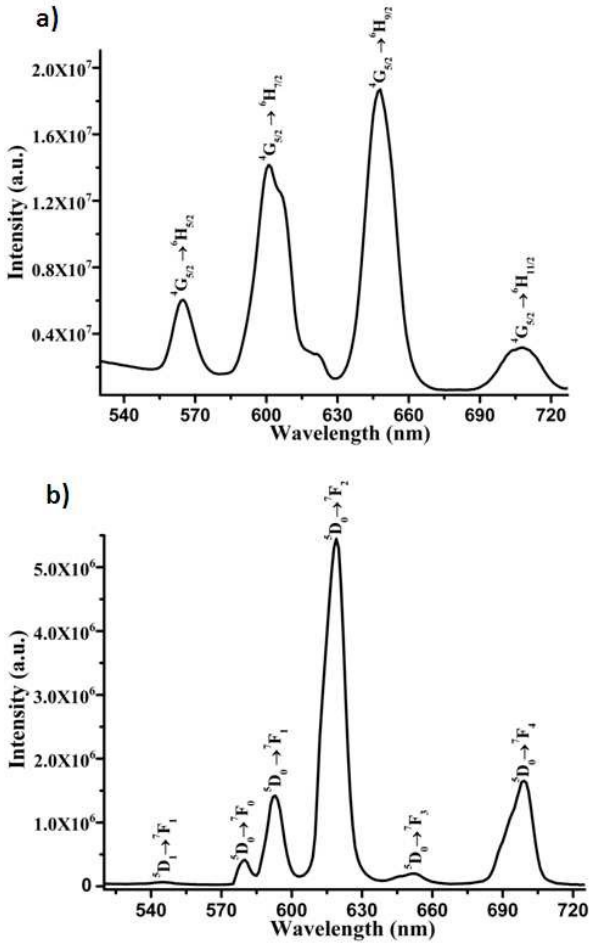

Fig. 7 Photoluminescence spectrum of (a) **Sm-5a** and (b) **Eu-6a** excited at 377 and 394 nm at room temperature.

In the emission spectrum of the **Ho-10a** compound, six emission peaks are observed at 466, 482, 498, 558, 652 and 660 nm in the visible region upon photo-excitation at 420 nm at room temperature. These peaks are assigned to the $^3D_3 \rightarrow {}^5I_8$, $^5F_2 \rightarrow {}^5I_8$, $^5F_3 \rightarrow {}^5I_8$, $^5S_2$, $^5F_4 \rightarrow {}^5I_8$, $^5F_5 \rightarrow {}^5I_8$ and $^3G_5 \rightarrow {}^5I_4$ transitions, respectively (see **fig. S12**).[22,53]

The **Er-11a** species exhibits green emission upon excitation at 380 nm at room temperature. There are six emission peaks at about 415 ($^2H_{9/2} \rightarrow {}^4I_{15/2}$), 442 ($^4F_{3/2} \rightarrow {}^4I_{15/2}$), 469 ($^4F_{5/2} \rightarrow {}^4I_{15/2}$), 515 ($^4F_{7/2} \rightarrow {}^4I_{15/2}$), 538 ($^2H_{11/2} \rightarrow {}^4I_{15/2}$) and 560 nm ($^4S_{3/2} \rightarrow {}^4I_{15/2}$) observed in the visible region, which are ascribed to f-f transitions. A green emission of **Er-11a** at 515 corresponds to the $^4F_{7/2} \rightarrow {}^4I_{15/2}$ transition of the Er^{III} ion (see **fig. S13**).[54] The **Tm-12a** compound shows two emission peaks at 456 and 483 nm upon photo-excitation at 358 nm at room temperature. These peaks are assigned to the $^1D_2 \rightarrow {}^3F_4$ and $^1G_4 \rightarrow {}^3H_6$ transitions of the Tm^{III} ion, respectively. The $^1D_2 \rightarrow {}^3F_4$ (456 nm) transition is responsible for the blue emission of **Tm-12a** compound. It is well known that the two electronic transitions of Tm^{III} are electric dipole allowed and their intensity is very sensitive both to the site symmetry and the chemical bonding of the Tm^{III} ions (see **fig. S14**).[55]

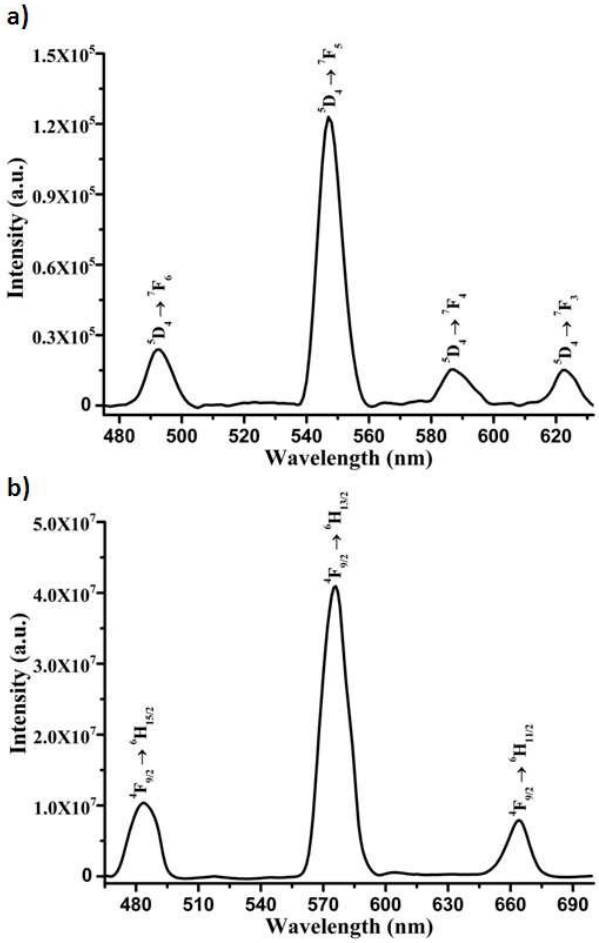

Fig. 8 Photoluminescence spectrum of (a) **Tb-8a** and (b) **Dy-9a** on excited at 330 and 370 nm at room temperature.

Thermogravimetric analysis

The thermal stabilities of the **La-1a** to **Sm-5a** molecular complexes were investigated in the temperature range 30-700 °C with a heating rate of 5 °C min^{-1} in a nitrogen atmosphere. The **La-1a** and **Ce-2a** species show single step weight loss which was attributed to the release of lattice water molecules from the crystal. The weight loss (%); calcd. for $27H_2O$ (found): 7.47 (7.55) in **La-1a** and for $28H_2O$: 7.72 (7.66) in **Ce-2a** took place in the temperature range 30-300 °C (see **fig. S15**). The TGA curves of the **Pr-3a** to **Sm-5a** molecular complexes exhibit two steps of weight loss which were associated to the loss of both crystal water molecules and acetate ligands bridging two NaK-[Ln-GeW_{11}] polyanions. The first step weight loss (%); calcd. for $25H_2O$ (found): 7.22 (7.09) in **Pr-3a**, for $22H_2O$: 6.47 (6.30) in **Nd-4a**, and for $19H_2O$: 5.69 (5.67) in **Sm-5a** were due to the loss of water molecules in the temperature range 30-300 °C. The second step weight loss (%);

calcd. (found): 1.88 (1.23) for **Pr-3a**, 1.88 (1.20) for **Nd-4a**, and 1.87 (1.18) for **Sm-5a** at a temperature up to ≈550 °C corresponded to the release of two acetate ligands from the polyanions (see **fig. S16**).

Magnetism

The magnetic properties of the **La-1a** to **Sm-5a** were investigated on a Microsence (ADE-EV9) vibrating sample magnetometer (VSM) in an applied magnetic field range of -22 to 22 kOe at 298 K. Magnetisation curves of all these compounds show ferromagnetic behaviour at room temperature (see **fig. S17**). Its interesting to note that La^{3+} ion has no unpaired electron but still exibits ferromagnetic character this may be due to spin-orbit coupling instead of magnetic exchange.

Electrochemistry

The electrochemical characterization of the ten molecular clusters **Pr-3a**, **Nd-4a**, **Sm-5a**, **Eu-6a**, **Tb-8a**, **Dy-9a**, **Ho-10a**, **Er-11a**, **Tm-12a** and **Yb-13a** based on the polytungstic fragment $[GeW_{11}O_{39}]^{8-}$ and on the acetate ligand was carried out in 1.0 M $LiCH_3COO + CH_3COOH$ media at pH 4, 5 and 6. By and large, the CVs obtained in the three media exhibit the same general features for all the compounds as far as the reduction processes assignable to the tungstencentres are concerned. The general pattern is a sequence of two reversible redox processes, the first one being 4-electron and the second one 2-electron. At pH 4, the two waves are not clearly separated, as shown by the black curve for **Sm-5a** (see **fig. 9**). Upon increasing the pH to 5 and 6 (red and blue CVs in **fig. 9**), the two waves progressively separate, the shoulder corresponding to the first wave at pH 4 becoming a distinct peak-shaped curve at pH 6. The standard midpoint potential values for the two waves, $E^{0,} = (E_{pa} + E_{pc})/2$, ($E_{pa}$ and E_{pc} being the oxidation and the reduction peak potentials, respectively) between pH 4 and 6 cathodically shift by 60 mV per pH unit for the first wave and by 80 mV per pH unit for the second wave (**Table 3**). Taking into account the Nernst equation, this implies that for the first redox process, the exchange of an electron encompasses the involvement of a proton, whereas for the second redox process this stoichiometry no longer applies. In fact, protons are electro-catalytically reduced in the potential range pertaining to the second wave. At even more negative potentials, beyond the second redox process, a rather large, irreversible wave is observed, corresponding both to the reduction of protons (solvent limit) and to the decomposition of the POM species into reduced blue compounds.

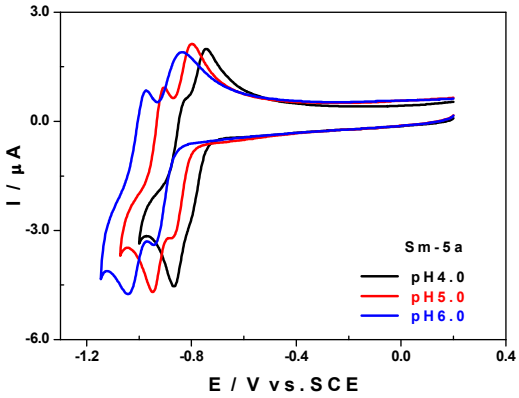

Fig. 9 CVs of **Sm-5a** in 1.0 M $LiCH_3COO + CH_3COOH$ / pH 4 (black), pH 5 (red) and pH 6 (blue). The scan starts in the direction of the negative potentials and reveals the waves attributed to the W^{VI} centers. Scan rate: 10 mV s^{-1}; working electrode: glassy carbon; counter electrode: Pt; reference electrode: SCE.

The CVs of the different compounds are very similar and are hardly affected by the replacement of a lanthanoid cation by another, as shown for **Sm-5a** and **Nd-4a** (see **fig. 10a**). However, when the response of the tungsten fragments $[GeW_{11}O_{39}]^{8-}$ present in each molecule is compared with that of one of the POMs (**Sm-5a** in **fig. 10b**), more pronounced differences in the peak positions and the wave shapes are observed. At pH 5 (**fig. 10b**), the separation between the two reduction steps is less clear on the CV of $[GeW_{11}O_{39}]^{8-}$, revealing a more pronounced basic character. Also, the reduction takes place at less negative potentials, with the same potential shift with respect to the waves of **Sm-5a** ($\Delta E_{c1} = \Delta E_{c2}$ = 30 mV).

Table 3. Cathodic peak potentials, E_{pc}, anodic peak potentials, E_{pa}, and standard midpoint redox potentials, $E^{0'} = (E_{pa} + E_{pc})/2$, for the W center reduction steps of **Sm-5a** in 1.0 M $LiCH_3COO + CH_3COOH$, from pH 4 to pH 6. The CVs were recorded at a scan rate of 10 mV s^{-1}; working electrode: glassy carbon; reference electrode: SCE.

Sm-5a (V vs. SCE)				
pH	4.0	5.0	6.0	ΔV / pH
E_{pc1}	**-0.800**	**-0.870**	**-0.950**	-
E_{pa1}	**-0.750**	**-0.800**	**-0.840**	-
$E_1^{0'}$	**-0.775**	**-0.835**	**-0.895**	**-0.060**
E_{pc2}	**-0.870**	**-0.950**	**-1.040**	-
E_{pa2}	**-0.820**	**-0.910**	**-0.970**	-
$E_2^{0'}$	**-0.845**	**-0.930**	**-1.005**	**-0.080**

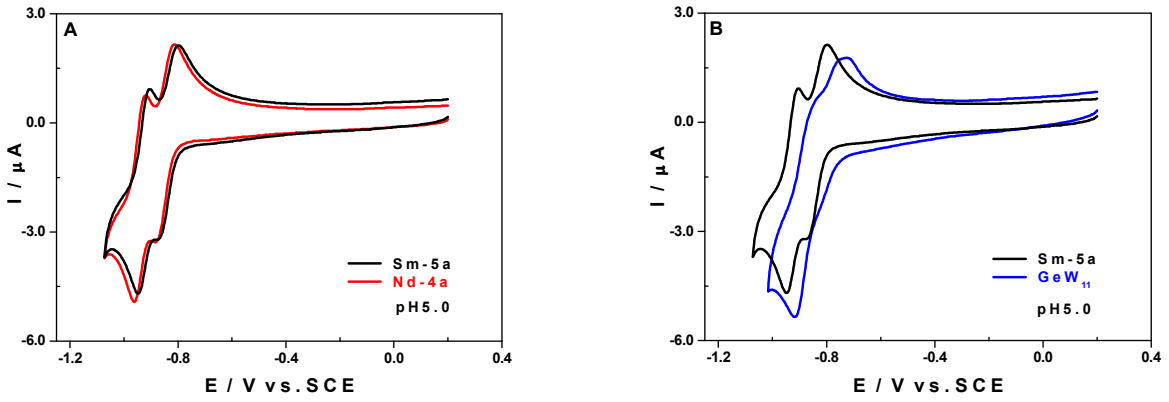

Figure 10.(a) CVs of **Sm-5a** (black) and **Nd-4a** (red); (b) CVs of **Sm-5a** (black) and **$[GeW_{11}O_{39}]^{8-}$** (blue) in 1.0 M $LiCH_3COO + CH_3COOH$ / pH 5. The scan starts in the direction of the negative potentials and reveals the waves attributed to the W^{VI} centers. Scan rate: 10 mV s^{-1}; working electrode: glassy carbon; counter electrode: Pt; reference electrode: SCE.

Conclusions

We have isolated sandwich type early lanthanoid substituted germanotungstates: $[Ln(\alpha\text{-}GeW_{11}O_{39})_2]^{13-}$ [Ln = La^{III}(**La-1**) and Ce^{III}(**Ce-2**)] and acetate bridged hybrid dimeric complexes of $[\{Ln(\mu\text{-}CH_3COO)GeW_{11}O_{39}(H_2O)\}_2]^{12-}$ [Ln = Pr^{III} (**Pr-3**), Nd^{III} (**Nd-4**) and Sm^{III} (**Sm-5**] by using single one pot reaction of trilacunary $Na_{10}[GeW_9O_{34}]\cdot 18H_2O$ precursor with $Ln(NO_3)_3\cdot nH_2O$ in a potassium acetate buffer at pH 4.7. All these compounds were structurally characterised by single crystal X-ray diffraction, FT-IR, ICP-AES, UV/vis, photoluminescence spectroscopy, thermogravimetric analysis, ^{13}C and ^{1}H NMR spectroscopy, magnetic analysis and electrochemistry. The chemistry of the early germanotungstates is different from that of the silicotungstates. We have also synthesised similar acetate-bridged complexes with mid and late lanthanoid cations according to previously reported procedure and characterized their photochromic properties. The **Pr-3a**, **Sm-5a**, **Eu-6a**, **Tb-8a**, **Dy-9a**, **Ho-10a**, **Er-11a** and **Tm-12a** compounds show good photoluminescence at room temperature. The magnetic studies of the **La-1a**, **Ce-2a**, **Pr-3a**, **Nd-4a** and **Sm-5a** were investigated at room temperature and show ferromagnetic behaviour. Electrochemistry allowed to assign two sequential 4-electron and 2-electron transfer waves to the W^{VI} centres of the POMs, whose behaviour is pH dependent, meaning that protons are also involved in the electron transfer steps.

Acknowledgements

F. H. gratefully acknowledges the University of Delhi for the financial support for this research work (R&D Grant). We thank the University Scientific Instrumentation Centre (USIC) and M.Tech Nano Science and Nano Technology (M.Tech-NSNT), University of Delhi, for providing instrumental facilities and IIT Bombay for ICP-AES. R. G. thanks CSIR, New Delhi for financial support.

References

1 M. T. Pope, in: *Heteropoly and IsopolyOxometalates*, Springer, Berlin, 1983.
2 M. T. Pope and A. Müller, *Angew. Chem. Int. Ed. Engl.*, 1991, **30**, 34; *Angew. Chem.*, 1991, **103**, 56.
3 C. L. Hill and C. M. Prosser-McCartha, *Coord. Chem. Rev*., 1995, **143**, 407.
4 I. V. Kozhevnikov, *Chem. Rev*., 1998, **98**, 171.
5 D. E. Katsoulis, *Chem. Soc. Rev.*, 1998, **98**, 359.
6 T. Yamase and M. T. Pope, (Eds.) *Polyoxometalates Chemistry for Nano-Composite Design*, Kluwer, Dordrecht 2002.
7 L. Cronin, in Compr. Coord. Chem. II, Ed. J. A. McCleverty and T. J. Meyer, Elsevier, Amsterdam, 2004, **7**, 1–57.
8 Z. F. Li, W. S. Li, X. J. Li, F. K. Pei, Y. X. Li and H. Lei, *Magn. Reson. Imaging*, 2007, **25**, 412.
9 U. Kortz, A. Müller, J. van Slageren, J. Schnack, N. S. Dalal and M. Dressel, *Coord. Chem. Rev.*, 2009, **253**, 2315.
10 R. D. Peacock and T. J. R. Weakley, *J. Chem. Soc. A.*, 1971, 1836.
11 R. D. Peacock and T. J. R. Weakley, *J. Chem. Soc. A.*, 1971, 1937.
12 J. Iball, J. N. Low and T. J. R. Weakley, *J. C. S. Dalton*, 1974, 2021.
13 K. Wassermann, M. H. Dickman and M. T. Pope, *Angew. Chem. int. Ed. Engl.*, 1997, **36**, 1445; *Angew Chem.*, 1997, **109**, 1513.
14 B. S. Bassil, M. H. Dickman, I. Römer, B. Kammer and U. Kortz, *Angew. Chem. Int. Ed.*, 2007, **46**, 6192; *Angew Chem.*, 2007, **119**, 6305.
15 (a) S. Reinoso, M. Giménez-Marqués, J. R. Galán-Mascarós, P. Vitoria, and J. M. Gutiérrez-Zorrilla, *Angew. Chem. Int. Ed.*, 2010, **49**, 8384; (b) B. Artetxe, S. Reinoso, L. S. Felices, J. M. Gutiérrez-Zorrilla, J. A. García, F. Haso, T. Liu, and C. Vicent, *Chem. Eur. J.*, 2015, **21**, 1.
16 F. Hussain, B. Spingler, F. Conrad, M. Speldrich, P. Kögerler, C. Boskovic and G. R. Patzke, *Dalton Trans.*, 2009, 4223.
17 F. Hussain, R. W. Gable, M. Speldrich, P. Kögerler and C. Boskovic, *Chem. Commun.*, 2009, 328.
18 F. Hussain, F. Conrad and G. R. Patzke, *Angew. Chem. Int. Ed.*, 2009, **48**, 9088; *Angew. Chem.*, 2009, **121**, 9252.
19 F. Hussain, A. Degonda, S. Sandriesser, T. Fox, S. S. Mal, U. Kortz and G. R. Patzke, *Inorg. Chim. Acta*, 2010, **363**, 4324.
20 F. Hussain and G. R. Patzke, *CrystEngComm.*, 2011, **13**, 530.
21 F. Hussain, S. Sandriesser, M. Speldrich and G. R. Patzke, *J. Solid State Chem.*, 2011, **184**, 214.
22 R. Gupta, M. K. Saini, F. Doungmene, P. de Oliveira and F. Hussain, *Dalton Trans.*, 2014, **43**, 8290.
23 M. K. Saini, R. Gupta, S. Parbhakar, A. K. Mishra, R. Mathur and F. Hussain, *RSC Adv.*, 2014, **4**, 25357.
24 M. K. Saini, R. Gupta, S. Parbhakar, S. Singh and F. Hussain, *RSC Adv.*, 2014, **4**, 38446.
25 R. Gupta, M. K. Saini and F. Hussain, *Eur. J. Inorg. Chem.*, 2014, 6031.
26 (a) X. Fang, P. Kögerler, Y. Furukawa, M. Speldrich and M. Luban, *Angew. Chem. Int. Ed.*, 2011, **50**, 5212; (b) A. R. de la Oliva, V. Sans, H. N. Miras, J. Yan, H. Zang, C. J. Richmond, D. Long and L. Cronin, *Angew. Chem. Int. Ed.*, 2012, **51**, 12759; (c) J. Gao, J. Yan, S. Beeg, D. Long and L. Cronin, *J. Am. Chem. Soc.*, 2013, **135**, 1796.
27 G. Hervé and A. Tézé, *Inorg. Chem.*, 1977, **16**, 2115.
28 C. Tourné, G. Tourné and M. Brianso, *Acta Cryst. Sect. B*, 1980, **36**, 2012.
29 C. Rong, J. Liu, X. Chen and E. Wang, *Inorg. Chim. Acta*, 1987, **130**, 265.
30 N. Jiang, L. Xu, F. Li, G. Gao and L. Fan, *Inorg. Chem. Comm.*, 2008, **11**, 24.
31 J. P. Wang, X. Y. Duan, X. D. Du and J. Y. Niu, *Cryst. Growth Des.*, 2006, **6**, 2266.
32 J. P. Wang, Q. X. Yan, X. D. Du, X. Y. Duan and J. Y. Niu, *Inorg. Chim. Acta*, 2008, **361**, 2701.
33 R. Khoshnavazi and S. Gholamyan, *J. Coord. Chem.*, 2010, **63**, 3365.
34 J. Miao, S. X. Zhang, S. J. Li, Y. H. Gao, X. Zhang, X. N. Wang and S. X. Liu, *J. Coord. Chem.*, 2011, **64**, 4006.
35 (a) S. Ping, M. FengJi and L. ShuXia, Chinese Science Bulletin, *Inorg. Chem.*, 2011, **56**, 2331; (b) W. D. Wang, X. X. Li, W. H. Fang and G. Y. Yang, *J. Clust. Sci.*, 2011, **22**, 87; (c) J. Zhao, D. Shi, L. Chen, Y. Li, P. Ma, J. Wang and J. Niu, *Dalton Trans.*, 2012, **41**, 10740; (d) H. Y. Zhao, J. W. Zhao, B. F. Yang, H. Hea and G. Y. Yang, *CrystEngComm.*, 2013, **15**, 8186; (e) J. Zhang, J. Li, L. Li, H. Zhao, P. Ma, J. Zhao and L. Chen, *Spectrochim Acta A*, 2013, **114**, 360 (f) J. W. Zhao, Y. Z. Li, F. Ji, J. Yuan, L. J. Chena and G. Y. Yang, *Dalton Trans.*, 2014, **43**, 5694; (g) H. Y. Zhao, J. W. Zhao, B. F. Yang, Q. Wei and G. Y. Yang, *J. Clust. Sci.*, 2014, **25**, 667.
36 P. Mialane, A. Dolbecq, E. Rivière, J. Marrot and F. Sécheresse, *Eur. J. Inorg. Chem.*, 2004, 33.
37 N. Vila, P. A. Aparicio, F. Sécheresse, J. M. Poblet, X. López and I. M. Mbomekalle, *Inorg. Chem.*, 2012, **51**, 6129.
38 Xcalibur CCD System; Oxford Diffraction Ltd: Abingdon, Oxfordshire, England, 2007

39 CrysAlis Pro software system, Version 171.32, Oxford Diffraction Ltd., Oxford, UK, 2007.
40 G. M. Sheldrick *Acta Cryst.* 2008, *A64*, 112-122, (b) G. M. Sheldrick, *Acta Cryst.* 2015, **C71**, 3–8
41 *SCALE3 ABSPACK*; CrysAlisPro, Version 1.171.36.32 Oxford Diffraction Ltd., Oxford, UK, 2013.
42 J. Niu, K. Wang, H. Chen, J. Zhao, P. Ma, J. Wang, M. Li, Y. Bai and D. Dang, *Cryst. Growth Des.*, 2009, **9**, 4362.
43 (a) I. D. Brown and D. Altermatt, *Acta Crystallogr., Sect. B*, 1985, **41**, 244; (b) A. Trzesowska, R. Kruszynski and T. J. Bartczak, *Acta Crystallogr., Sect. B*, 2004, **60**, 174.
44 C. Craciun and L. David, *J. Alloys Comp.*, 2001, **323/324**, 743.
45 (a) H. Naruke, J. Iijima and T. Sanji, *Inorg. Chem.*, 2011, **50**, 7535; (b) T. Som and B. Karmakar, *Spectrochim. Acta Part A*, 2011, **79**, 1766; (c) K. Binnemans and C. G. Walrand, *Chem. Phys. Lett.*, 1995, 235, 163.
46 F. S. Liu, Q. L. Liu, J. K. Liang, J. Luo, L. T. Yang, G. B. Song, Y. Zhang, L. X. Wang, J. N. Yao and G. H. Rao, *J. Lumin.*, 2005, **111**, 61.
47 L. Ni, F. Hussain, B. Spingler, S. Weyeneth and G. R. Patzke, *Inorg. Chem.*, 2011, **50**, 4944.
48 M. Ayvacikli, A. Ege, S. Yerci and N. Can, *J. Lumin.*, 2011, **131**, 2432.
49 (a) L. Yang, X. Xu, L. Hao, X. Yang, J. Tang and R. Xie, *Opt. Mater.*, 2011, **33**, 1695; (b) B. Zhou, L. Tao, Y. H. Tsang, W. Jin and E. Y. B. Pun, *Opt. Express.*, 2012, **20**, 3803.
50 X. Y. Zhao, S. X. Liu, Y. H. Ren, J. F. Cao, R. G. Cao and K. Z. Shao, *J. Solid State Chem.*, 2008, **181**, 2488.
51 (a) D. D. Liu, Y. G. Chen, C. J. Zhang, H. X. Meng, Z. C. Zhang and C. X. Zhang, *J. Solid State Chem.*, 2011, **184**, 1355; (b) W. A. Pisarski, J. Pisarska, R. Lisiecki, Ł. Grobelny, G. D. Dzik and W. R. Romanowski, *J. Lumin.*, 2011, **131**, 649.
52 W. F. Zhao, C. Zou, L. X. Shi, J. C. Yu, G. D. Qian and C. D. Wu, *Dalton trans.*, 2012, **41**, 10091.
53 (a) S. Bhushan and A. Oudhia, *Ind. J. Pure Applied Phys.*, 2009, **47**, 60; (b) X. Li, S. Gai, C. Li, D. Wang, N. Niu, F. He and P. Yang, *Inorg. Chem.*, 2012, **51**, 3963.
54 (a) A. A. Andreev, *Phys. Solid State*, 2002, **44**, 248; (b) X. Li, S. Gai, C. Li, D. Wang, N. Niu, F. He and P. Yang, *Inorg.Chem.*, 2012, **51**, 3963; (c) G. S. R. Raju, J. Y. Park, H. C. Jung, E. Pavitra, B. K. Moon, J. H. Jeong, J. S. Yu, J. H. Kim and H. Choi, *J. Alloys Comp.*, 2011, **509**, 7537.
55 (a) S. Wang, S. Su, S. Song, R. Deng and H. Zhang, *CrystEngComm.*, 2012, **14**, 4266; (b) S. Sailaja, S. J. Dhoble, C. N. Raju and B. S. Reddy, *Physica B*, 2012, **407**, 103.